Synthesis, spectroscopic characterization, antimicrobial and antitumor studies of mono-, bi- and tri-nuclear metal complexes of a new Schiff base ligand derived from o-acetoacetylphenol

Omima M.I. Adly [a, *], Magdy Shebl [a], Hoda F. El-Shafiy [a], Saied M.E. Khalil [a], A. Taha [a], Mohammed A.N. Mahdi [a, b]

[a] Chemistry Department, Faculty of Education, Ain Shams University, Roxy, Cairo 11341, Egypt
[b] Department of Industrial Chemistry, Faculty of Applied Science, Hajjah University, Yemen

ABSTRACT

New mono-, bi- and trinuclear metal complexes of Cr(III), Mn(II), Fe(III), Co(II), Ni(II), Cu(II), Zn(II), Cd(II) and UO_2(VI) with a new Schiff base ligand H_3L; ((E)-2-hydroxy-N'-(4-(2-hydroxyphenyl)-4-oxobutan-2-ylidene)) benzohydrazide (H_3L) have been synthesized. The ligand and its metal complexes were characterized by elemental analyses, IR, ^{1}H NMR, electronic, ESR and mass spectra, conductivity and magnetic susceptibility measurements as well as thermal analyses. The metal complexes exhibited octahedral and tetrahedral geometrical arrangements. Kinetic parameters (E_a, A, ΔH, ΔS and ΔG) of the thermal decomposition stages have been evaluated using Coats—Redfern equations. Structural parameters of the synthesized compounds were calculated on the basis of DFT level implemented in the Gaussian 09 program and Hyperchem 7.52 and correlated with the experimental data. The antimicrobial activity of the present compounds was screened against Gram—positive bacteria (Staphylococcus aureus and Bacillus subtilis), Gram—negative bacteria (Salmonella typhimurium and Escherichia coli), yeast (Candida albicans) and fungus (Aspergillus fumigatus). The antitumor activity of the ligand and its Ni(II) and Cu(II) complexes was investigated against HepG2 cell line.

1. Introduction

A large number of 1,3-diacarbonyl compounds are of the great interest in the synthesis of metal complexes with broad spectrum of pharmaceutical activity [1,2]. 1,3-diacarbonyl compounds are good precursors for the synthesis of a diversity of Schiff bases and hydrazones through reactions with a variety of amines and hydrazines [3,4]. These ligands and their metal complexes have different applications in different fields such as bioinorganic chemistry, material science, catalysis, separation and encapsulation processes, hydrometallurgy, formation of compounds with unusual properties and metal—metal interactions [5—8]. Metal complexes of these Schiff bases have numerous applications including antibacterial, antifungal [9—11] antitumor [12] anticonvulsant [13] anti-HIV [14] and antiviral activities [15,16]. They can be used as an

efficient materials in the polymerization reactions, functional dyes and pigments, medical and pharmaceutical areas [17,18]. Several applications have been related for these complexes in chemical analysis [19], absorption and transport of oxygen [20] and in pesticides [21]. There is great interest about multi-dentate ligands because their binding selectively can be altered subtly by having the ligand enforce a specific spatial arrangement of donor atoms [22].

The aim of work is to synthesize a new Schiff base ligand, ((E)-2-hydroxy-N'-(4-(2-hydroxyphenyl)-4-oxobutan-2-ylidene)) benzohydrazide, and its metal complexes with chromium(III), manganese(II), iron(III), cobalt(II), nickel(II), copper(II), zinc(II), cadmium(II) and dioxouranium(VI) ions. The structures of the ligand and its metal complexes were characterized by using elemental and thermal analyses, IR, ^{1}H NMR, electronic, ESR and mass spectra in addition to magnetic susceptibility and conductivity measurements. Kinetic parameters of the thermal decomposition stages have been evaluated using Coats-Redfern equations. Molecular modeling was carried out for the ligand and its

* Corresponding author.
E-mail address: omima_adly@yahoo.com (O.M.I. Adly).

complexes and the results were correlated with the experimental data. The antimicrobial activity of the ligand and its complexes was screened against selected kinds of bacteria and fungi. Finally, the antitumor activity of the ligand and its Ni(II) and Cu(II) complexes was investigated against HepG2 cell line.

2. Experimental

2.1. Materials

o-Acetoacetylphenol and 2-hydroxybezohydrazied were prepared following the literature procedures [23,24]. Metal acetates, metal indicators, EDTA disodium salt, ammonium hydroxide and nitric acid were either BDH or Merck chemicals. Organic solvents were reagent grade chemicals and were used without further purification.

2.2. Synthesis of ((E)-2-hydroxy-N′-(4-(2-hydroxyphenyl)-4-oxobutan-2-ylidene)) benzohydrazide (H₃L)

The new Schiff base (Scheme 1) was prepared by adding o-acetoacetylphenol (2 g, 11.22 mmol) dissolved in absolute ethanol (40 mL) to 2-hydroxybezohydrazied (1.71 g, 11.22 mmol) in absolute ethanol (40 mL). The reaction mixture was stirred for 6 h and a yellow precipitate is formed upon cooling the solution to room temperature. The product was filtered off and washed with few amounts of ethanol then diethylether, air-dried and recrystallized from ethanol and the yield was 1.7 g (91%). The analytical and physical data of the ligand (Scheme 1) and its metal complexes are listed in Table 1.
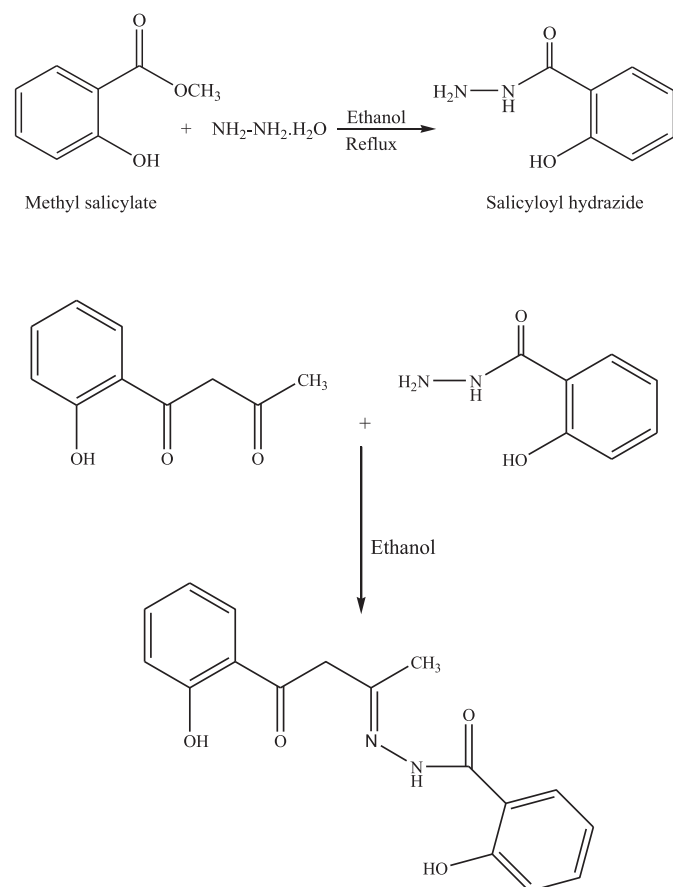
2.3. Synthesis of the metal complexes

A hot 30 mL ethanolic solution of the metal salt was gradually added to the solution of the ligand (40 mL) in 1:2 (L: M) molar ratio. The mixture was heated under reflux for 7 h during which the solid complex precipitated. The precipitate was filtered off, washed with ethanol or methanol then diethyl ether and finally air-dried and stored in an evacuated desicator over anhydrous calcium chloride. The following representative examples are given in details.

2.3.1. [(H₃L)Ni(OAc)(H₂O)₂].0.5C₂H₅OH, 5

To 0.5 g (1.60 mmol) of the ligand dissolved in 30 mL ethanol, was added 0.797 g (3.20 mmol) of Ni(OAc)₂·4H₂O dissolved in 30 mL ethanol with stirring. The reaction mixture was heated under reflux for 7 h. The precipitate was filtered off, washed with ethanol then ether and finally air-dried. Yield: 0.5 g (65%).

2.3.2. [(H₂L)(UO₂)₂(OAc)₂], 9

To 0.5 g (1.60 mmol) of the ligand dissolved in 30 mL methanol, was added 1.358 g (3.20 mmol) of UO₂(OAc)₂·2H₂O dissolved in 30 mL methanol with stirring. The reaction mixture was heated under reflux for 7 h. The precipitate was filtered off, washed with methanol then ether and finally air-dried. Yield: 0.5 g (31%).

2.4. Analytical and physical measurements

Elemental analyses were carried out using Vario El-Elementar at the Ministry of Defense, Chemical War Department in Egypt. Analyses of the metals followed the same procedure as described previously. Analyses of the metals followed decomposition of their complexes with concentrated nitric acid. The resultant solution was diluted with bidistilled water and filtered. The solution was then neutralized with aqueous ammonia solution (except iron(III) complexes) and the metal ions titrated with EDTA [25–27]. IR spectra were recorded using KBr discs on FT IR Nicolet 6700 spectrometer. Electronic spectra were recorded as solutions in DMF or Nujol mulls on a Jasco UV–Vis spectrophotometer model V-550 UV–Vis. ¹H NMR spectra were recorded at room temperature by using a Bruker WP 200 SY spectrometer. Dimethylsulfoxide, DMSO-d_6, was used as a solvent and tetramethylsilane (TMS) as an internal reference. The spectra were extended from 0 to 18 ppm. The chemical shifts (δ) are given down field relative to TMS. D₂O was added to every sample to test for the deuteration of the samples. ESR spectra of the complexes were recorded at an Elexsys, E500, Bruker company. However, the mass spectra were recorded at 70 eV on a Gas chromatographic GCMSqp 1000 ex Shimadzu instrument. The magnetic susceptibility measurements were carried out at room temperature using a magnetic susceptibility balance of the type Johnson Matthey, Alfa product, Model No. (MKI). Effective magnetic moments were calculated from the expression $\mu_{eff.} = 2.828\ (\chi_M.T)^{1/2}$ B.M., where χ_M is the molar susceptibility corrected using Pascal's constants for the diamagnetism of all atoms in the compounds [28]. Molar conductivities of 10^{-3} M solutions of the solid complexes in DMF were measured on the Corning conductivity meter NY 14831 model 441. The TG–DTG measurements were carried out on a Shimadzu thermogravimetric analyzer in dry nitrogen atmosphere and a heating rate of 20 ℃/min using the TA-50 WS1 program.

2.5. Antimicrobial activity

The standardized disc-agar diffusion method [29,30] was followed to determine the activity of the synthesized compounds against the sensitive organisms Staphylococcus aureus (ATCC 25923) and Bacillus subtilis (ATCC 6635) as Gram positive bacteria,

Scheme 1. Formation of H₂L, ligand.

Table 1
Analytical and physical data for transition metals complexes of H_3L ligand.

No.	Reaction	Complex M. F. [F. Wt]	Color	Yield (%)	M.P °C	Elemental analysis, % found/(calc.)			
						C	H	N	M
	H_3L	$[(H_3L)][312.32]$ $C_{17}H_{16}N_2O_4$	Yellow	91	188	64.40 (65.37)	5.05 (5.16)	9.02 (8.97)	—
1	H_3L + Cr(OAc)$_3$·H$_2$O	$[(HL)Cr(OAc)_4(H_2O)_4]. 0.5H_2O$ $C_{25}H_{34}N_2O_{16.5}Cr_2 [730.06]$	Brown	75	>300	40.94 (41.13)	4.10 (4.69)	3.76 (3.83)	14.85 (14.21)
2	H_3L + Mn(OAc)$_2$·4H$_2$O	$[(HL)Mn_2(OAc)_2]$ $C_{21}H_{20}N_2O_8Mn_2 [538.26]$	Orange	90	>300	45.97 (46.86)	3.73 (3.74)	4.64 (5.20)	20.01 (20.41)
3	H_3L + Fe(NO$_3$)$_3$·9H$_2$O	$[(L)Fe_3(NO_3)_6(H_2O)_6].2H_2O$ $C_{17}H_{29}N_8O_{30}Fe_3 (993.447)$	Brown	75	>300	20.46 (20.55)	2.92 (2.94)	11.33 (11.28)	16.90 (16.91)
4	H_3L + Co(OAc)$_2$·4H$_2$O	$[(H_3L)Co_2(OAc)_4(H_2O)_4] C_{25}$ $H_{36}N_2O_{16}Co_2 [738.42]$	Yellowish brown	82	>300	39.79 (40.66)	3.43 (4.91)	3.81 (3.79)	15.30 (15.96)
5	H_3L + Ni(OAc)$_2$·4H$_2$O	$[(H_3L)Ni(OAc)(H_2O)_2].0.5C_2$ $H_5OHC_{20}H_{25}N_2O_{8.5}Ni [488.10]$	Greenish yellow	65	>300	49.62 (49.21)	4.20 (5.16)	5.78 (5.73)	11.75 (12.06)
6	H_3L + Cu(OAc)$_2$·H$_2$O	$[(H_3L)Cu(OAc)_2]$ $C_{21}H_{22}N_2O_8Cu [493.95]$	Olive green	65	>300	48.93 (51.06)	4.27 (4.48)	6.63 (5.67)	12.71 (12.86)
7	H_3L + Zn(OAc)$_2$·2H$_2$O	$[(H_2L)Zn(OAc)]$ $C_{19}H_{18}N_2O_6Zn [435.35]$	Yellow	85	>300	51.90 (52.42)	4.10 (4.16)	6.60 (6.43)	14.30 (14.93)
8	H_3L + Cd(OAc)$_2$.2H$_2$O	$[(H_3L)_2Cd].5H_2O$ $C_{34}H_{40}N_4O_{13}Cd [824.71]$	Yellow	50	>300	49.18 (49.52)	4.19 (4.89)	6.85 (6.79)	13.08 (13.58)
9	H_3L + UO$_2$(OAc)$_2$.2H$_2$O	$[(H_2L)(UO_2)_2(OAc)_2].H_2O$ $C_{21}H_{22}N_2O_{13}U_2 [986.41]$	Brown	75	>300	25.36 (25.57)	2.23 (2.24)	3.00 (2.84)	—

Salmonella typhimurium (ATCC 14028) and *Escherichia coli* (ATCC 25922) as Gram negative bacteria and *Candida albicans* (ATCC 10231) and *Aspergillus fumigatus* as fungus strain. The antibiotic chloramphenicol was used as reference in the case of Gram-positive bacteria, cephalothin in the case of Gram-negative bacteria and cycloheximide in the case of fungi.

2.6. Antitumor activity

Cell toxicity was monitored on HepG2 cells by determining the effect of the test samples on cell morphology and cell viability according to literature method [31].

3. Results and discussion

The IR spectrum of the free ligand exhibited three characteristic bands at 3437, 1628 and 1558 cm^{-1} that may be assigned to v(O—H), v(C=N) and v(C===O) + v(C===C) groups, respectively (Table 2) [4].

Electronic spectral data of the ligand in DMF (Table 3) displayed two bands at 34,843 and 23,041 cm^{-1}. The first band may be due to

n-π* transitions of the azomethine linkage and the aromatic benzene ring. The second band may be assigned to n-π* transitions of the C=O group and/or charge transfer transitions within the molecule.

^{1}H NMR spectrum of the free ligand, dissolved in DMSO-d_6, presented in Fig. 1, showed two signals at 11.79 and 13.42 ppm, which may be assigned to phenolic OH protons, (Scheme 1). The two signals observed at 10.88 and 10.38 ppm may be assigned to NH protons in tautomer I (Scheme 2). Signal observed at 2.21 may be assigned to methyl protons. The aromatic protons were observed in the range of 6.79–7.94 ppm. Based on NMR spectral data, it was concluded that the ligand exists as tautomers I and II in solution.

The mass spectrum of the free ligand showed the molecular ion peak at *m/z* 312 confirming its formula weight (F.W 312.32). The mass fragmentation pattern, presented in Scheme 3, supported the suggested structure of free ligand (Scheme 1).

3.1. Metal complexes

Reactions of the current ligand with Cr(III), Mn(II), Fe(III), Co(II),

Table 2
Characteristic IR spectral data of the ligand H_3L and its transition metals complexes chelates.

No.	Complexes	IR Spectra (cm)$^{-1}$							
		v(OH) H$_2$O/EtOH/ phenolic	vNH	vC=N	vC=== O+vC ===C	vC===N	vM-O	vM-N	Other bands
	H_3L	3437	3254 (3286)^a	1628 (1616)	1558 (1578)	1480,	—	—	1334 (1346), 1292 (1267), 1224 (1208), 1162 (1195), 1070 (1065)
1	$[(HL)Cr(OAc)_4(H_2O)_4]. 0.5H_2O$	3406	3270	1606	1563	1451	594	—	1687; v_{as} (COO$^-$), 1398; v_s (COO$^-$); (monodentate OAc)
2	$[(HL)Mn_2(OAc)_2]$	3426	3285	1591	1567	1450	531	—	1600; v_{as} (COO$^-$), 1496; v_s (COO$^-$); (bidentate OAc)
3	$[(L)Fe_3(NO_3)_6(H_2O)_6].2H_2O$	3373	—	1603	1568	1510	593	483	1383, 1146; v(NO$_3^-$) (monodentate)
4	$[(H_3L)Co_2(OAc)_4(H_2O)_4]$	3376	3260	1590	1560	1424	560	—	1680; v_{as} (COO$^-$), 1345; v_s (COO$^-$); (monodentate OAc)
5	$[(H_3L)Ni(OAc)(H_2O)_2]0.5C_2H_5OH$	3410	3294	1599	1564	1499	532	463	1683; v_{as} (COO$^-$), 1394; v_s (COO$^-$); (monodentate OAc)
6	$[(H_3L)Cu(OAc)_2]$	3470	3183, 3063	1599	1521	1501	540	446	1620; v_{as} (COO$^-$), 1376; v_s (COO$^-$); (monodentate OAc)
7	$[(H_3L)Zn(OAc)]$	3429	3252	1600	1549	1502	549	430	1588; v_{as} (COO$^-$), 1379; v_s (COO$^-$); (monodentate OAc)
8	$[(H_3L)_2Cd].5H_2O$	3463	3281	1606	1566	1496	532	466	—
9	$[(H_2L)(UO_2)_2(OAc)_2].H_2O$	3272	3190	1601	1574	1468	503	—	1601; v_{as} (COO$^-$), 1497; v_s (COO$^-$); (bidentate OAc) and 912; v(O=U=O)

^{a} Vibrational bands in paranthesis computed on the basis of semiemperical PM3 level by means of Hyperchem 7.52.

Table 3
Electronic spectra, magnetic moments and molar conductivity data of the H_3L ligand and its complexes.

No.	Complex	Electronic spectral bands[a] (nm)	μ_{compl}[d] B.M.	$\mu_{eff.}$[e] B.M.	Conductance[b] (Ω^{-1} cm^2 mol^{-1})
	H_3L	$(34,843,23,041)$[b]	–	–	12.5
1	$[(HL)Cr(OAc)_4(H_2O)_4]. 0.5H_2O$	$(22,371,21,834,17,301)$[c]	6.50	3.82	6.80
2	$[(HL)Mn_2(OAc)_2]$	$20,576$[a] $(22,172,20,576,19,960,16806)$[c]	7.23	5.11	31.60
3	$[(L)Fe_3(NO_3)_6(H_2O)_6].2H_2O$	$19,608, 18,450, 17,636$[a]	8.17	4.72	32.80
4	$[(H_3L)Co_2(OAc)_4(H_2O)_4]$	$21,413, 19,268$[a]	8.12	5.74	13.50
5	$[(H_3L)Ni(OAc)(H_2O)_2].0.5C_2H_5OH$	$(31,250, 24,450, 22,831, 17,482)$[c]	3.18	–	26.70
6	$[(H_3L)Cu(OAc)_2]$	$(16,313)$[b]	2.20	–	9.44
7	$[(H_3L)Zn(OAc)]$	$(24,570,21,930)$[c]	–	–	20.70
8	$[(H_3L)_2Cd].5H_2O$	$(24,691,22,371,21,186)$[c]	–	–	22.30
9	$[(H_2L)(UO_2)_2(OAc)_2].H_2O$	$(24,630,20,746)$[c]	–	–	8.75

[a] Nujol mull.
[b] Solutions in DMF (10^{-3} M).
[c] Concentrated solutions.
[d] $\mu_{compl.}$ is the total magnetic moments of all cations in the complex.
[e] $\mu_{eff.}$ is the magnetic moment of one cationic species in the complex.

Ni(II), Cu(II), Zn(II), Cd(II) and UO_2(VI) ions, in the molar ratio 1:2 (L: M), yielded mono-, bi- and trinuclear complexes. The prepared complexes are stable at room temperature, non-hygroscopic and insoluble in water and most common organic solvents. The elemental analyses of the metal complexes agreed well with the proposed formulae (Table 1).

3.1.1. IR spectra

The IR spectral data of the metal complexes are listed in Table 2. The IR spectra of the complexes were compared with that of the free ligand in order to resolve the coordination sites that may be involved in chelation. There are some guide peaks in the spectrum of the ligand, which were helpful in achieving this goal. Comparison of the IR spectra of the metal complexes with that of the free ligand revealed that the broad band around 3437 cm^{-1} which was assigned to ν(OH) stretching modes in H_3L was observed in the spectra of all complexes with higher broadness in the range 3272–3470 cm^{-1}. This influence was attributed to the effect of coordination of hydroxyl oxygen and/or coordinated or uncoordinated water molecules associated with the complexes. The presence of coordinated or uncoordinated water molecules were confirmed by elemental and thermal analyses. The band assigned to ν(C═O) + ν(C═C) at 1558 cm^{-1} exhibits red shift in the range 9–37 cm^{-1} for Cu(II), UO_2(II), Co(II) Zn(II), and Ni(II)- complexes, suggesting the participation of the carbonyl oxygen in chelation [32]. However, Cr(III), Fe(III), Mn(II) and Cd(II) complexes display a blue shift to higher frequencies in the range 5–10 cm^{-1}. This might understanding in the light of HSAB (hard soft acid base) concept, some metal ions prefer coordination with oxygen centers and other favored nitrogen coordinating centers. This interpretation supported by the negative slope of ν(C═O) versus ν (M–O); ν M–O = $-1818.2-0.820$ νC═O, r = 0.96, n = 5, except (**1**, **2**, **4** and **7**) i.e., increasing the strength of M–O bond order accompanied by elongation of C═O (decrease the bond strength according to Gutmann's bonds variation rules) [33].

The azomethine group ν(C═N) band which appeared as a medium peak at 1628 cm^{-1} in the spectrum of the ligand appeared at lower wavenumber for some complexes in the range 22–54 cm^{-1}. Nevertheless, δ(C–N) deformation mode (1480 cm^{-1}) displays a red shift in the range 7–56 cm^{-1} for all the complexes, except for Mn(II)- and Ni(II)-complexes which has higher frequency 1496 and 1499 cm^{-1}, respectively compared with that of the free ligand. This approves in the participation of the azomethine group of the enol form (see Scheme 2) in chelation [34]. This consequence confirmed by the linear relationship of ν(C═N) with

ν(M–N), νM-N = 1304.3–0.591 νC═N, r = 0.94, n = 6, except (**3**, **5** and **8**). The negative slope emphasized that increasing the M–N bond strength go along with the bond weakness of C═N. Moreover, the new bands appeared in the ranges 503–594 and 426-483 cm^{-1} those assigned to ν(M–O) and ν(M–N), respectively [35–37].

Complexes **1** and **4 -7** showed new bands at (1687–1588) and (1389–1345) cm^{-1} which may be assigned to ν_{asym}(COO$^-$) and ν_{sym}(COO$^-$) of the acetate group. The difference between the two bands indicates the monodentate nature of the acetate group [38–40]. On the other hand, complexes **2** and **9** showed new bands characteristic for ν_{asym}(COO$^-$) and ν_{sym}(COO$^-$) of the acetate group in (1600 and 1601) and (1496 and 1497) cm^{-1}, respectively. The difference between the two bands (104 cm^{-1}) indicates a bidentate fashion of the acetate group [38–40]. Complex **3**, displayed new bands at 1383 and 1146 cm^{-1}, which may be assigned to the monodentate NO$_3^-$ group [41,42]. The dioxouranium(VI) complex **9** showed a strong band at 912 cm^{-1}, which may be assigned to the ν_3(UO_2) [35,36,43]. The value of ν_3 is utilized to calculate the force constant (F) of (O═U═O) by using McGlynn and Smith relation [44]. The calculated force constant is 6.867 mdyn/Å. The U–O distance is also calculated by using Jones relation [45]. The value of R_{U-O} is 1.738 Å. The calculated F_{U-O} and R_{U-O} values are consistent with the reported range for the uranyl complexes [46].

The molar conductivity values of the metal complexes at room temperature (Table 3) are in the range 6.8–32.8 Ω^{-1} cm^2 mol^{-1} indicating that all complexes have non electrolytic nature [47]. This finding is consistent with the infrared spectral data that showed the coordinated nature of acetate and nitrate anions.

3.1.2. Electronic spectra and magnetic moment measurements

The electronic spectral data of the metal complexes in DMF solution and/or Nujol mull, and magnetic moment at room temperature are listed in Table 3.

Comparison of the UV–Vis spectra of the current metal complexes with that of the free ligand, showed the persistence of the ligand bands in all complexes. However, the bands were slightly shifted to blue or red regions of the spectrum in all complexes. Also, new bands were observed in the spectra of the complexes which are listed in Table 3.

The electronic spectrum of Cr(III) complex **1** showed three absorption bands in the visible region at 22371, 21834 and 17301 cm^{-1} those assigned to MLCT, $^4T_{2g}(F) \leftarrow {}^4A_{2g}(F)$ and $^4T_{1g}(F) \leftarrow {}^4A_{2g}(F)$ of transitions of the octahedral geometry [48,49]. Whereas the third transition band which is due to $^4T_{1g}(P) \leftarrow {}^4A_{2g}(F)$ transition lies in the range of the ligand transitions that predicted at

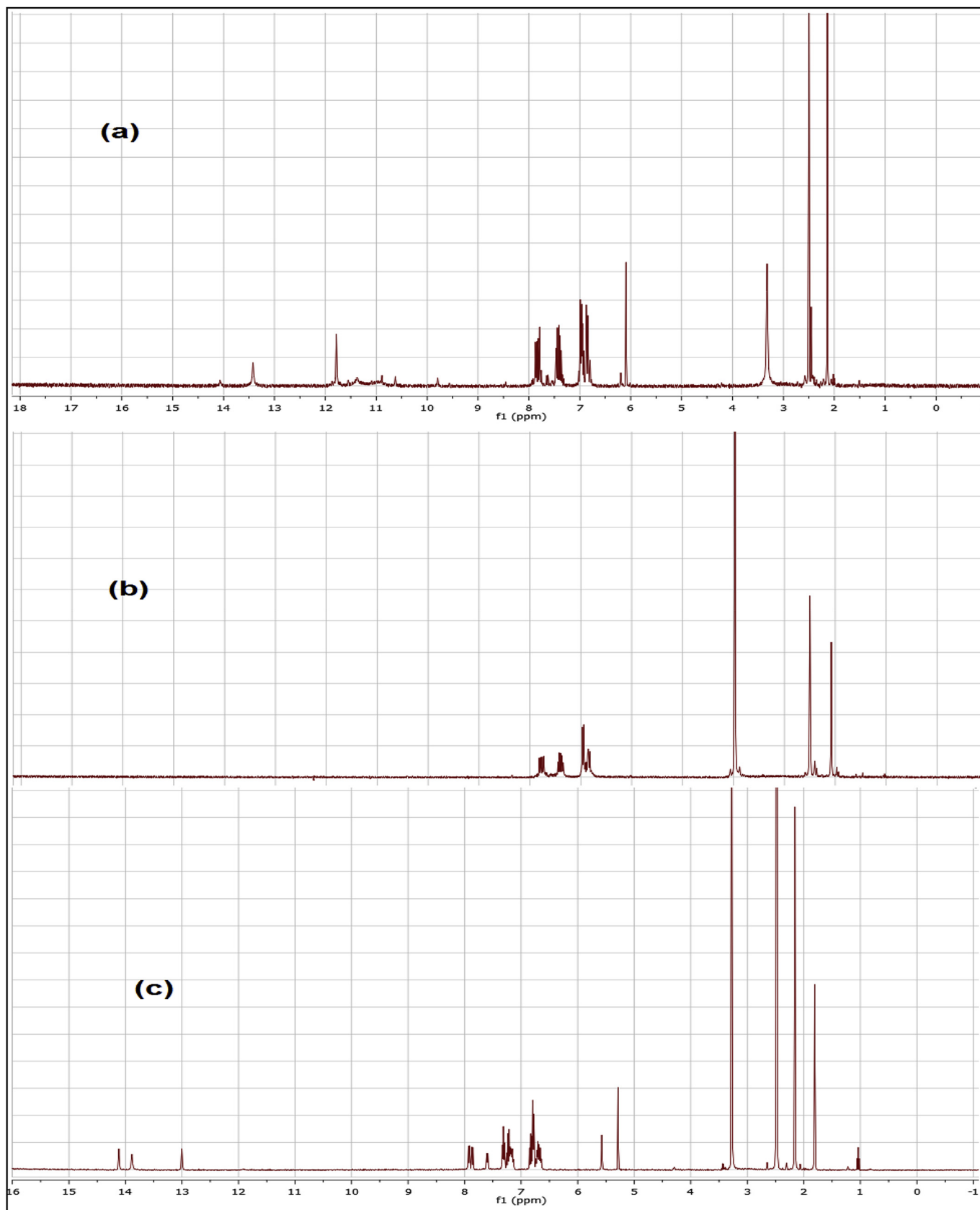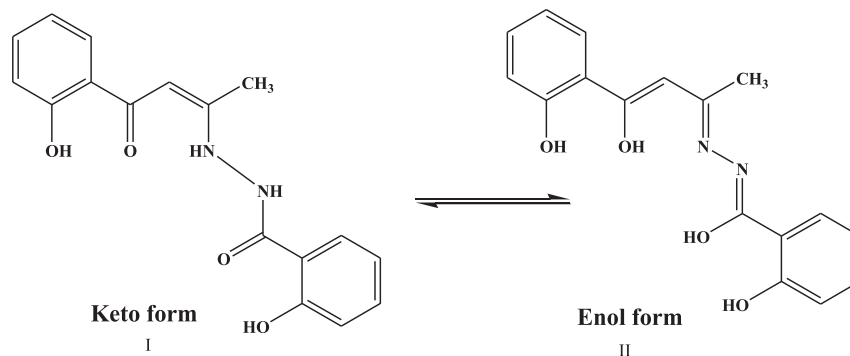**Fig. 1.** ^{1}H NMR spectra (δ, ppm) in DMSO-d_6 solvent of: (a) H$_2$L ligand without addition of D$_2$O, (b) H$_2$L ligand after the addition of D$_2$O and (c) [[(H$_3$L) Zn(OAc)] complex **7**.

Scheme 2. Keto and enol forms of the Schiff base, H_3L, ligand.

36287 cm^{-1}. The ligand field parameters of the Cr(III) complex in progress has been calculated using Tanab–Sugano diagrams B (414.5 cm^{-1}), 10Dq (1730 cm^{-1}) and β (0.40). The measured magnetic moment value found to be 3.82 B.M analogues to the spin-only of three unpaired electrons.

The spectrum of Mn(II) complex **2** showed a series bands at 22173, 20576, 19960 and 16807 cm^{-1}, these bands assigned to $^4A_{1g}(G) \leftarrow {}^2T_{2g}$, $^4T_{1g}(E) \leftarrow {}^2T_{2g}$, $^4T_{2g}(G) \leftarrow {}^2T_{2g}$ and $^4T_{1g}(G) \leftarrow {}^2T_{2g}$ transitions, respectively, which corresponds to a tetrahedral structure. The calculated ligand field parameters of the current Mn(II) complex are found to be: B (575.5 cm^{-1}), 10Dq (10935 cm^{-1}) and β (0.60). The magnetic moment has low of Mn(II) complex (5.11 B.M) due to metal–metal interaction [50].

The electronic spectrum of Fe(III) complex **3** showed three absorption bands at 19608, 18450 and 17637 cm^{-1}. The former band

Scheme 3. Mass Fragmentation pattern of Schiff base, H_3L, ligand.

could be assigned to a charge transfer band and the later bands can be assigned to $^2A_{1g}(I) \leftarrow {}^2T_{2g}$ and $^2T_{2g}(F) \leftarrow {}^2T_{2g}$ electronic transition [51]. The value of the magnetic moment of complex **3** is 4.72 B.M., which is less than expected for octahedral Fe(III) complexes (5.92 B.M.), suggesting an equilibrium between the high spin and low spin octahedral species in the ratio 79.73% [52].

The electronic spectrum of Co(II) complex **4** exhibits two bands at (21413, 19268 cm^{-1}). The first band at 21413 cm^{-1} might assigned $^4T_{1g}$ (P) $\leftarrow {}^4T_{1g}$ (F),(v_3), whereas the second band at 19268 cm^{-1}. $^4A_{2g}$ (F) $\leftarrow {}^4T_{1g}$ (F) (v_2) assigned to the transition, suggesting that there is an octahedral geometry around the Co(II) ion. This emphasized by the magnetic moment value, $\mu_{eff} = 5.74$ B.M, the higher value may be due to orbital contribution, that related to high spin octahedral geometry around cobalt(II) ion [42,53]. The v_1 band not observed, but it can be intended and found at 9132 cm^{-1}. The calculated ligand field parameters were B (263 cm^{-1}), 10Dq (913 cm^{-1}) and β (0.27), within the range reported for octahedral structure [52].

The UV–Vis spectrum of Ni(II)-complex **5** exhibits four bands 31250, 24450, 22831 and 17482 cm^{-1}. The higher energy band, 31250 cm^{-1} assigned to n-π* and the band at 24450 cm^{-1} suggested for MLCT. Whereas the other two bands assigned to $^3T_{1g}(F) \leftarrow {}^3A_{2g}(F)$ and $^3T_{1g}(P) \leftarrow {}^3A_{2g}(F)$ transitions, representing octahedral structure [53]. This finding was further emphasized by the measured magnetic moment at 3.18 B.M., which lies in the range (2.9–3.3 B.M) of the Ni(II) octahedral complexes [54]. The spectral data provide the ligand field parameters: B (501 cm^{-1}), 10Dq (8654 cm^{-1}) and β (0.46), and the first transition band, $^3T_{2g}$ (F) $\leftarrow {}^3A_{2g}$ (F), in the spectrum predicted at 37129 cm^{-1}.

The electronic spectrum of the Cu(II) complex **6** showed one band at 16,313 cm^{-1} that may be assigned to ($^2E_g \leftarrow {}^2T_{2g}$) transition corresponding to distorted octahedral geometry [55]. The effective magnetic moments of the Cu(II) complex is 2.20 B.M., which is consistent with one unpaired electron (d^9) [53]. This interpretation supported by the X-band ESR spectrum of the Cu(II) complex, that recorded in the solid state at 25 °C. The spectrum exhibits one broad band (Fig. 2) with g$_\perp$ = 2.05 and g$_\parallel$ = 2.30 the profile of the spectrum is consistent with the octahedral geometry [56].

The Zn(II) **7** and Cd(II) **8** complexes are diamagnetic as expected and display two absorption bands for Zn(II) **7** at 24570 and 21930 cm^{-1}; and 24691, 22371 and 21186 cm^{-1} for Cd(II) **8** complex. These bands might attribute to π → π * and n→ π * transitions in the vicinity of the Schiff base ligand, in addition to MLCT transition.

The electronic spectrum of UO$_2$(VI) complex **9** showed two absorption bands at 24631 and 20767 cm^{-1}, just similar to that found for Zn(II) complex **7**. The lower energy band might arises from
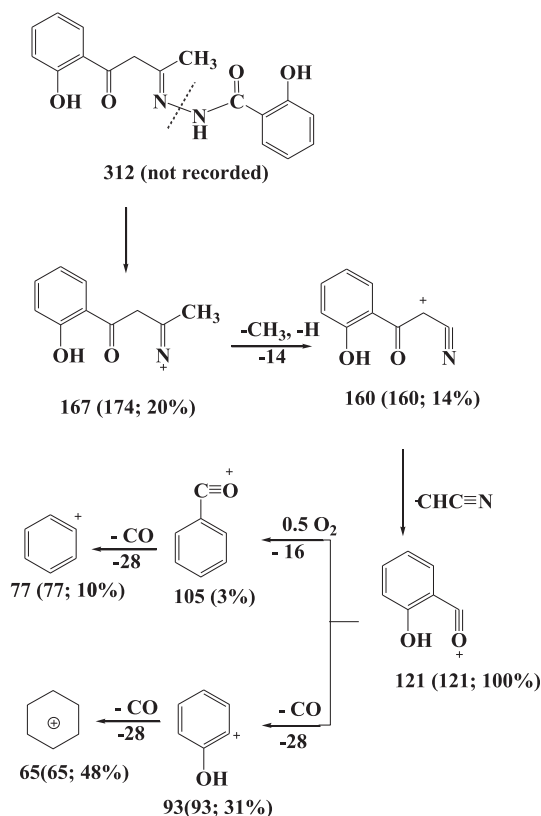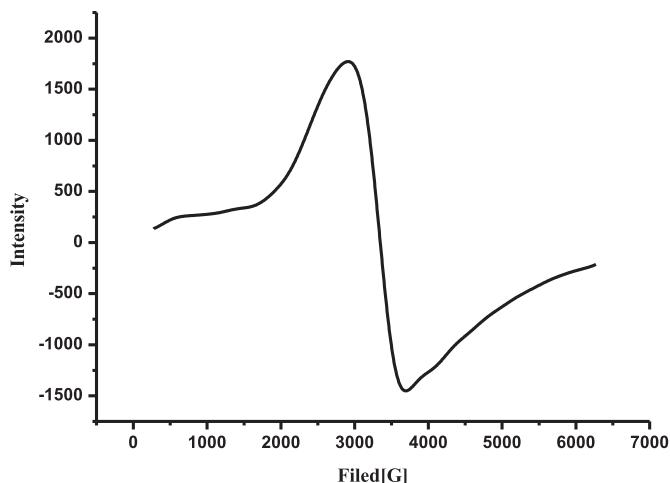
Fig. 2. ESR spectra of [(H$_3$L)Cu(OAc)$_2$] complex 6.

Fig. 4. TGA curves of [(H$_3$L)Ni(OAc)(H$_2$O)$_2$].0.5C$_2$H$_5$OH 5.

metal → ligand charge transfer (MLCT) and/or apical oxygen →Fº (U) [57]. However the other band in the UV region could be attributed to n→ π* electronic transition in the vicinity of ligand The magnetic moment measurement of the UO$_2$(VI) complex 9 refers to the diamagnetic behavior as expected.

3.1.3. Thermal analysis

The simultaneous thermal gravimetric analysis (TGA) of metal complexes studied from ambient temperature to 800 °C in nitrogen atmosphere were depicted in Figs. 3–5. TGA help to explore the associated water or solvent molecules to be in the inner or outer coordination sphere of the central metal ion. Complexes 1, 2, 4, 5, 6 and 9 were taken as representative examples for thermal analysis. The results of thermal analysis were summarized in Table 4, the data given are in good agreement with the theoretical formulae suggested from elemental analyses.

The thermogram of Cr(III) complex 1 exhibited that the compound exhibited three decomposition stages. The first stage in the temperature range 46–101 °C, which correspond to the weight loss of half non-coordinated water molecule (weight loss; Calc./Found%; 1.12/1.11). The second stage in the temperature range 103–180 °C, which match to the loss of two-coordinated water molecules (weight loss; Calc./Found%; 4.87/5.18). However, the third stage which occurred between 180 and 434 °C, which correspond to the loss of two-coordinated water molecules and half CH$_3$COOH molecule (weight loss; Calc./Found%; 8.94/8.88).

The thermogram of complex 4 showed two weigh losses in the ranges 45–190 °C and 190–510 °C. The first stage observed at DTG pe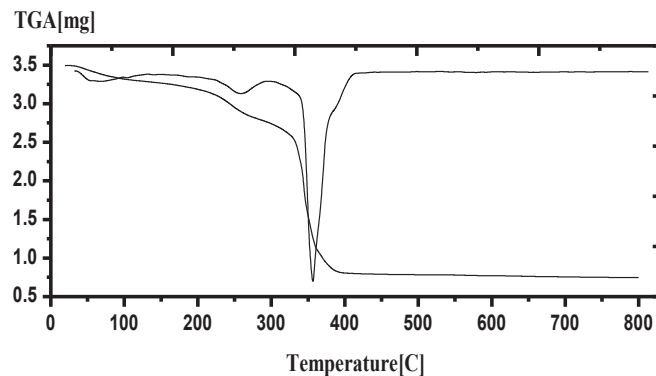ak = 114 °C that corresponding to four coordinated water molecules (weight loss; Calc./Found%; 16.25/16.05). The second stage at DTG peak = 393 °C which analogues to the loss of three CH$_3$COOH molecules (weight loss; Calc./Found%; 24.44/24.30).

The thermogram of complex 5 shows three decomposition stages, 20–70 °C, 84–279 and 280–799 °C. The first stage corresponds to half non-coordinated ethanol molecule (weight loss; Calc./Found%; 4.74/4.17). The second stage in the temperature which suggest loss of two coordinated water and half CH$_3$COOH molecules (weight loss; Calc./Found%; 13.72/13.83). The last stage in the temperature range 280–799 °C, which analogues to the loss of half CH$_3$COOH and C$_{14}$H$_{10}$N$_2$O$_3$ molecules (weight loss; Calc./Found%; 59.20/59.04).

In order to access the influence of the type of the metal on the thermal behavior of the complexes, the order n, and the activation parameters of the various decomposition stages were determined from the TG thermograms using the Coats-Redfern equations [52].

The order (n) and thermo kinetic parameters: activation energy (E$_a$), enthalpy (ΔH^*), entropy (ΔS^*) and free energy changes (ΔG^*) of the thermal degradation of the complexes are are calculated as described elsewhere and tabulated in (Table 5) [34]. Inspection of the data in Table 5 advocate, the following remarks:

The negative values of ΔS^* indicate that the activated complex is more ordered than the reactants and/or the reactions are slow [58]. This interpretation emphasized by the negative slope of the linear relationship of E$_{gap}$ versus ΔS^*, E$_{gap}$/eV = −6.43−0.058 ΔS^*, r = 0.97, n = 5 all TGA points included. i.e., increasing the calculated energy gap (vide infra) that reveal high stable complex was accompanied by more ordered complex (-ve ΔS^*). Furthermore, the negative slope of the computed E$_{LUMO}$ (measures the stability of the complex) with the entropy changes; E$_{LUMO}$/eV = −3.75−0.012 ΔS^*,
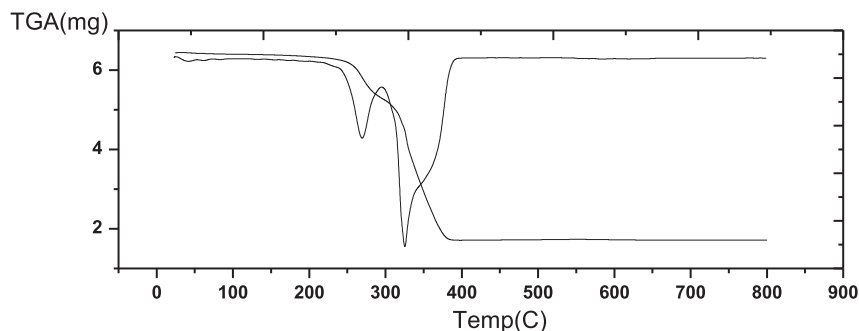

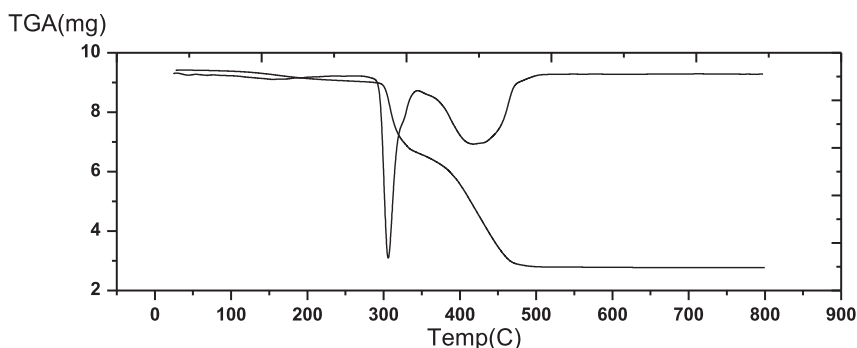Fig. 3. TGA curves of [(HL)Mn$_2$(OAc)$_2$] 2.

Fig. 5. TGA curves of [(H3L)Cu(OAc)2] **6**.

Table 4
Thermal gravimetric results of the H_3L ligand and its metal complexes.

Compound	DTG peak (°C)	Temperature range (°C)	Decomposition product lost (formula weight)	Weight loss (%) found (calculated)
[(HL)Cr(OAc)$_4$(H$_2$O)$_4$]. 0.5H$_2$O **1**	80	46–103	$-0.5H_2O$	1.11 (1.21)
	134	103–180	$-2H_2O$	5.18 (4.87)
	359	180–434	$-2H_2O+0.5CH_3COOH$	8.88 (8.94)
[(HL)Mn$_2$(OAc)$_2$] **2**	270	221–296	$-CH_3COOH + CO$	16.05 (16.29)
	339	297–391	$-CH_3COOH + C_{14}H_{13}N_2O_2$	55.38 (55.71)
[(H$_2$L)Co$_2$(OAc)$_4$] **4**	114	45–190	$-4H_2O$	9.30 (9.70)
	393	190–510	$-3 CH_3COOH$	24.44 (24.30)
[(H$_3$L)Ni(OAc)(H$_2$O)$_2$].0.5C$_2$H$_5$OH **5**	60	20–70	$-0.5C_2H_5OH$	4.17(4.71)
	246	84–279	$-2H_2O+ 0.5CH_3COOH$	13.83 (13.72)
	346	280–799	$-0.5CH_3COOH + C_{14}H_{10}N_2O_3$	59.20 (59.04)
[(H$_3$L)Cu(OAc)$_2$] **6**	312	292–345	$-2CH_3COOH$	25.05(24.84)
	419	345–475	$-C_{11}H_{12}O_3N_2$	43.92(44.65)
[(H$_2$L)(UO$_2$)$_2$(OAc)$_2$].H$_2$O **9**	85	47–153	$-H_2O$	1.85 (1.83)
	406	154–605	$-CH_3COOH + CO$	8.14 (8.92)
	736			

r = 0.98, n = 4 except Cu(II)-complex, supported decreasing of entropy with the increasing of the complex stability. Consequently, the rate of decomposition decreases with the increasing of the stability of complexes [59]. Additionally, the positive slope of the relationship of computed ΔH_f against ΔS^*, $\Delta H_f = 1.92$ e5 $+ 846.1$ ΔS^*, r = 0.999, n = 3 except Cr(II)- and Cu(II)-complexes, reveals again that less stable complex (high ΔH_f) is easier to decompose (less $-$ve values of ΔS^*).

The positive values of ΔH^* mean that the decomposition stages are endothermic. Increasing the stability of complex, leads to decreases the binding coordination sphere with the hydrated water molecules, so they will be easier to remove from the outer sphere. This interpretation emphasized by the $-$ve slope of E_{gap}/eV versus

ΔH^*; $E_{gap} = 9.67-0.072 \Delta H^*/kJ.mol^{-1}$, r = 0.996, n = 4, except Cu(II)-complex. This means that increasing the stability of complex (high E_{gap}) accompanied by effortless dehydration of water molecules.

The positive sign of ΔG^* values indicates autocatalytic effect of metal ions on the thermal decomposition of the complexes and non$-$spontaneous processes.
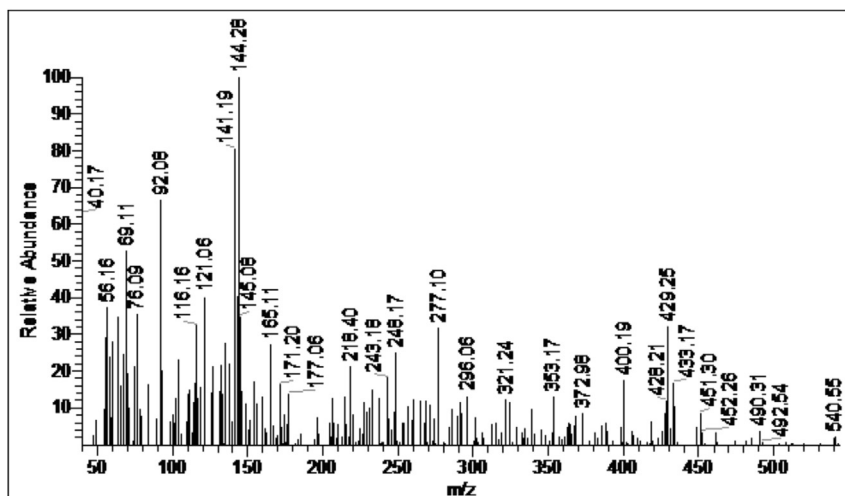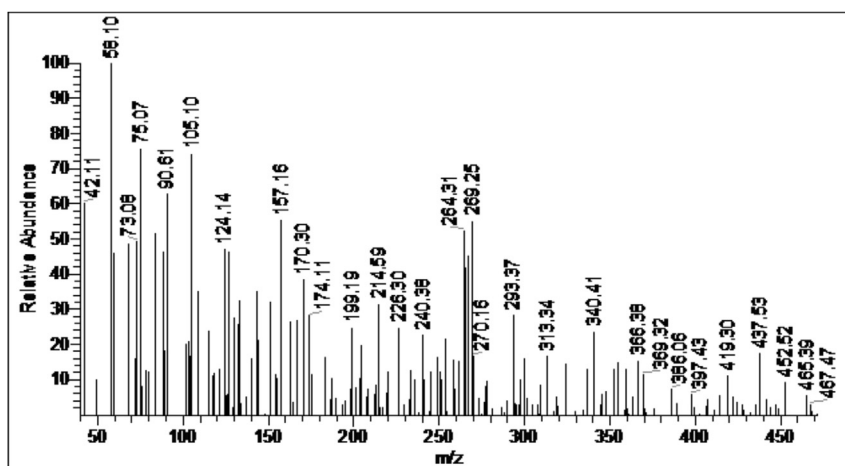
3.1.4. Mass spectra

The molecular ion peaks observed in the mass spectra of free ligand and some complexes **2**–**5**, **8** and **9** taken as representative examples are confirmed their proposed formulae. Figs. 6 and 7 depicts the mass spectra of complexes **2** and **5** and the mass

Table 5
Temperature of decomposition, and the kinetic of metal complexes.

Complexes	Step	T (K)	A (S^{-1})	E (kJ mol^{-1})	ΔH (kJ mol^{-1})	ΔS (kJ mol-1K^{-1})	ΔG (kJ mol^{-1})
[(HL)Cr(OAc)$_4$(H$_2$O)$_4$]. 0.5H$_2$O **1**	First	353	31.09	29.40	26.63	- 0.094221	33.287
	Second	407	22.46	61.71	58.33	- 0.22994	93.640
	Third	631	68280.59	92.53	87.29	- 0.1669	102.41
[(HL)Mn$_2$(OAc)$_2$] **2**	First	543	154939.97	121.135	161.62	- 0.15885	86.416
	Second	613	46.587	44.896	39.80	- 0.22728	139.36
[(H$_2$L)Co$_2$(OAc)$_4$] **4**	First	387	73.29	8.16	4.92	- 0.21972	85.04
	Second	666	45.17	43.48	37.95	-0.22823	152.04
(H$_3$L)Ni(OAc)(H$_2$O)$_2$].0.5C$_2$H$_5$OH **5**	First	333	26.539	24.851	22.082	- 0.22688	75.573
	Second	519	37.671	35.983	31.67	- 0.22766	118.19
	Third	619	2.616×10^{11}	205.19	200.043	- 0.0407	25.408
[(H$_3$L)Cu(OAc)$_2$] **6**	First	585	1.3243×10^{19}	283.787	278.923	0.107234	62.453
	Second	692	84.95	86.466	80.715	- 0.22329	154.597
[(H$_2$L)(UO$_2$)$_2$(OAc)$_2$].H$_2$O **9**	First	357	6.774	5.088	2.120	- 0.23882	89.559
	Second	679	10.557	8.871	3.226	- 0.24047	163.285

Fig. 6. Mass spectrum of [(HL)Mn₂(OAc)₂] **2**.

Fig. 7. Mass spectrum of [(H₃L)Ni(OAc)(H₂O)₂].0.5C₂H₅OH **5**.

fragmentation pattern of complex **2** shown in Scheme 4. Complexes **2** and **4** showed the molecular ion peaks at m/z 540 and 738 respectively which agree well with the formula weights of the non-hydrated or non-solvated complexes; [(HL)Mn₂(OAc)₂] and [(H₂L)Co₂(OAc)₄(H₂O)₄]. This agrees the proposed formulae of these complexes as 2:1; M:L. However, complexes **3, 5, 8** and **9** displayed the molecular ion peaks at m/z 964, 488, 827 and 986, respectively are in consistent with the proposed formulae weights calculated for [(HL)Fe₃(NO₃)₆(H₂O)₆].2H₂O, [(H₃L)Ni(OAc)(H₂O)₂]. 0.5C₂H₅OH, [(H₃L)₂Cd].5H₂O and [(H₂L)(UO₂)₂(OAc)₂].H₂O complexes, confirming with 1:3, 1:1, 2:1 and 1:2; M:L stoichiometry.

3.1.5. ¹H NMR spectra

¹H NMR spectral data of the metal complexes Zn(II),Cd(II) and UO₂(IV) dissolved in DMSO-d_6, given in Fig. 1 and summarized in Table 6 exhibited signals at (13.88,14.12) and (13.87,15.41) ppm in Zn(II) and Cd(II) respectively, which may be assigned to two phenolic OH protons which indicate that OH group indicating that OH group don't participate in the coordination. In UO₂(IV) complex only one OH proton was appeared in the spectrum at 13.68 ppm and the other one was not observed indicating its participation in the coordination. The two signals observed at 13.00, 12.4 and11.71 ppm may be assigned to NH protons (tautomer II is

dominant) (Scheme 2). Signals observed at 5.28, 5.41 and 6.06 in Zn(II), Cd(II) and UO₂(IV) respectively attributed to CH=CN (olofinic proton) and this confirm that the tautomer II is more predominant in the solution while in the solid state the tautomer I is predominant (Scheme 2).

Based on the above interpretation of different analytical and spectral data, the proposed structures of the metal complexes are represented in Fig. 8.

4. Molecular orbital calculations

The molecular structures were elucidated on the basis of the spectral, molar conductance, magnetic susceptibility and TGA data which designated that the octahedron geometry for the current complexes. All molecular calculations were performed in the gas phase for the elucidated structures of the free ligand and its metal complexes except uranyl-complexes **9** (see Figs. 9–12). The free ligand has been geometrically optimized by means of Density Functional Theory (DFT) using the B3LYP and the basis set 6-31G level, provides by the Gaussian 09 program. However, the metal complexes are geometrically optimized, on the basis of *PM3* level using semi-empirical implemented on Hyperchem *7.52* program as a result of the complication of the presence of metal ion and higher
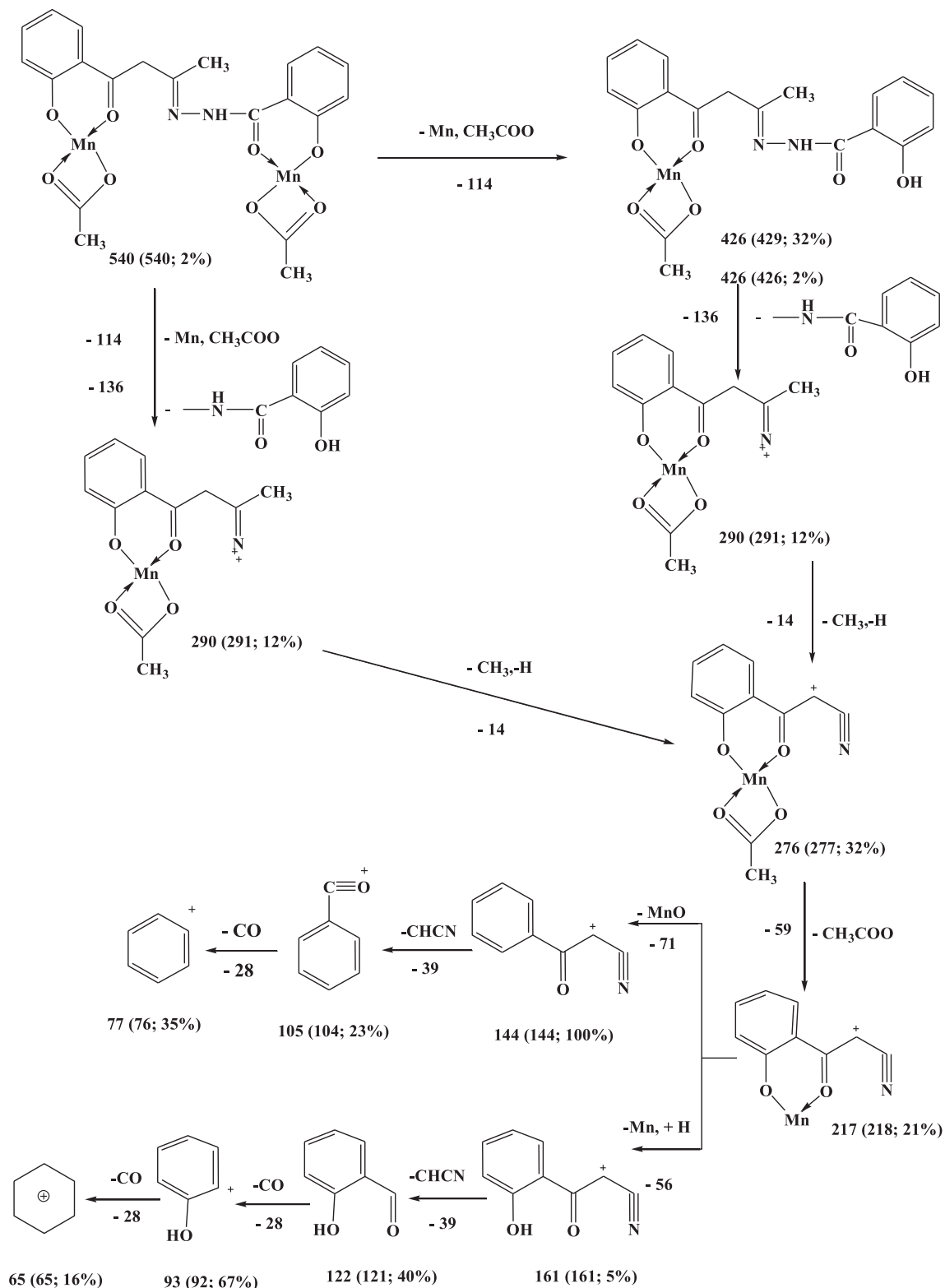
Scheme 4. Mass fragmentation of Mn(II) complex **2**.

molecular mass, which requires unavailable workstation in our lab. The utility of quantum chemical descriptors such as heat of formation, dipole moment and frontier molecular orbitals (highest occupied molecular orbital and lowest unoccupied molecular orbitals energies) are collected in Table 7 in elucidating the structure

of the current compounds.

The frontier molecular orbital (FMO) contribution is very important in determining the charge-separated states of the studied molecules because the relative ordering of occupied and virtual orbital provides a reasonable qualitative indication of

Table 6
^{1}H NMR spectra of the Schiff base, H$_2$L, ligand and its Cd(II), Zn(II) and UO$_2$(VI) complexes.

Keto form   **Enol form**
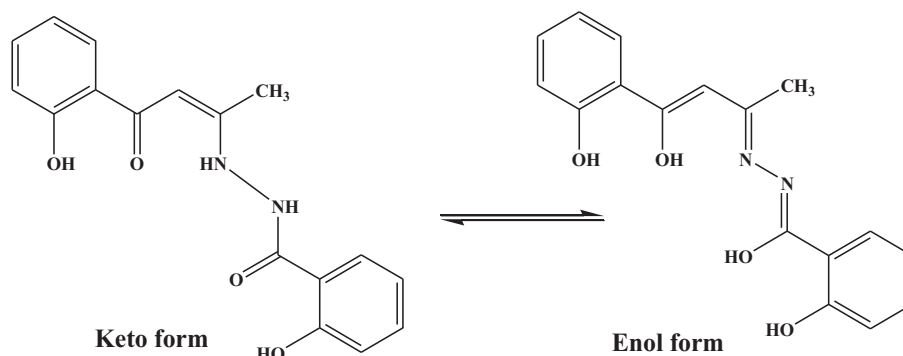
^{1}H NMR Chemical shifts in ppm

H$_2$L ligand	Zn(II) complex **7**	Cd(II) complex **8**	UO$_2$(IV) complex **9**	Assignment
2.21	2.51	2.18	2.31	(s, 3H, CH$_3$)
3.32				(s, 2H, CH)
5.28	5.28	5.41	6.06	(s, 1H, CH)
6.79–6.89	6.64–7.13	6.64–6.73	6.75–7.08	(m,2H, Ar-H)
6.92–6.99	7.15–7.23	7.08–7.16	7.21–7.58	(m,2H, Ar-H)
7.31–7.55	7.58–7.60	7.56–7.58	7.70–7.81	(m,2H, Ar-H)
7.76–7.94	7.85–7.93	7.75–7.84	7.94–7.99	(m,2H, Ar-H)
10.88	13.00	12.4	11.71	(bs,1H, NH) exchangeable with D$_2$O)
11.38				(bs,1H NH exchangeable with D$_2$O)
11.78,13.42	13.88,14.12	13.87,15.41	13.68	(bs,2H, 2OH exchangeable with D$_2$O)

excitation properties and provides also the ability of electron hole transport [48]. The energies of the frontier molecular orbitals of studied molecules are given in Table 7. A comparison between the bond lengths of the ligand and its metal complexes was demonstrated in Table 8. It is well known that the HOMO and LUMO energies and energy gaps are weightly relative to optical and electronic properties.

The detailed data of absolute energy of the frontier orbital calculated by DFT for the free ligand. The distributions and energy levels of the HOMO-2 (−6.569 eV), HOMO-1(-5.930 eV), HOMO (−5.212 eV), LUMO (−1.659 eV), LUMO+1 (−1.074 eV) and LUMO+2 (−0.272 eV) orbitals were computed at the B3LYP/6-31G level for the current ligand. Both the highest occupied molecular orbitals (HOMOs) and the lowest-lying unoccupied molecular orbitals (LUMOs) are mainly localized on the rings of both sides as shown in the contour plots of the frontier orbitals of the free ligand Fig. 13 (HOMO& LUMO density), indicating that the HOMO are mostly the π-antibonding type orbitals. The HOMO orbitals are mainly delocalized on the o-acetoacetyl moiety and Schiff base linkage part, while the LUMO orbitals are mainly delocalized on phenyl rings of both sides. Namely, electron transitions are corresponding to the n-π* and π - π* electron transitions. The value of the energy separation between the HOMO and LUMO for the free ligand (3.55 eV) and this low energy gap indicates that the current ligand is potentially interesting for electronic transitions.

It is well established that HOMO orbitals account for the Lewis basicity [49], whereas LUMO orbitals characterize the Lewis acidity. According to the frontier molecular orbital approximation, high value of E_{HOMO} infers that the molecule or ligand can easily release electrons to the unoccupied orbital of the metal ion, indicating strong Lewis base [49]. However, high E_{LUMO} suggest that the metal ion can easily accept electrons from the occupied orbital of the ligand, indicating strong binding affinity. Furthermore, the extent of Lewis Acid-Base interaction of the current compounds analogues to E_{gap} values ($E_{gap} = E_{LUMO}$- E_{HOMO}) which are linearly correlated

with the stretching vibrational frequencies of νC=O, E_{gap}/eV = 255.56−0.1617 νC=O/cm^{-1}, r = 0.98, n = 4, except: Mn(II), Cu(II), Zn(II) and Cd(II)-complexes. The negative slope emphasized that, increase the stability of the complex accompanied by the elongation of the carbonyl group (hypsochrmic shift of the vibrational frequency). However, ΔH_f/Kcal/mol = −5816 + 37.152 νC=O/cm^{-1}, r = 0.96, n = 5 except **1**, **2**, **6**, **8** and **9** complexes. The positive slope indicates again that increasing of heat of formation, $\underline{\Delta H_f}$ (relevance to weak stability of complex) lead to blue shift of the vibrational frequency of νC=O bond (weak interaction of the carbonyl group toward the metal ion). Furthermore, comparison between the bond lengths of the free ligand coordinating centers and their corresponding values in its metal complexes (Table 8) demonstrates elongation of the coordinating centers after coordination (C=O$_{a1}$, 1.216 (free ligand) − 1.502 A^o) (Fe(III)-complex and C=N$_1$ 1.301(free ligand − 1.519 A^o (Cd(II)-complex)), which agree well with the Gutmann's bonds variation rules [33].

The vibrational analysis of the current free ligand (H$_3$L) is performed on the basis of the characteristic vibrations of functional groups modes. The vibrational frequencies calculated given in parenthesis have been summarized in Table 2. Comparison between the calculated and the observed vibrational spectra helps us to understand the observed spectral features. Comparison of the frequencies calculated by B3LYP with experimental values reveals the overestimation of the calculated vibrational modes due to neglect of anharmonicity in real system. Inclusion of electron correlation in density functional theory to a certain extent makes the frequency values smaller in comparison with experimental values. The linear relationship between the experimental and the calculated characteristic IR bands, νExp/cm^{-1} = 1.013 νCalc/cm^{-1} -18.74, R^2 = 0.999, supports the assignments of the characteristic IR bands.

Furthermore, the linear correlation between the calculated dipole moment (μ) versus the vibrational frequency of ν_{M-O}, μ/D = −84.119 + 0.209 ν_{M-N}/cm^{-1}, r = 0.973, n = 7, except **1** and **9** complexes. The positive slopes put forward increase of the μ-values
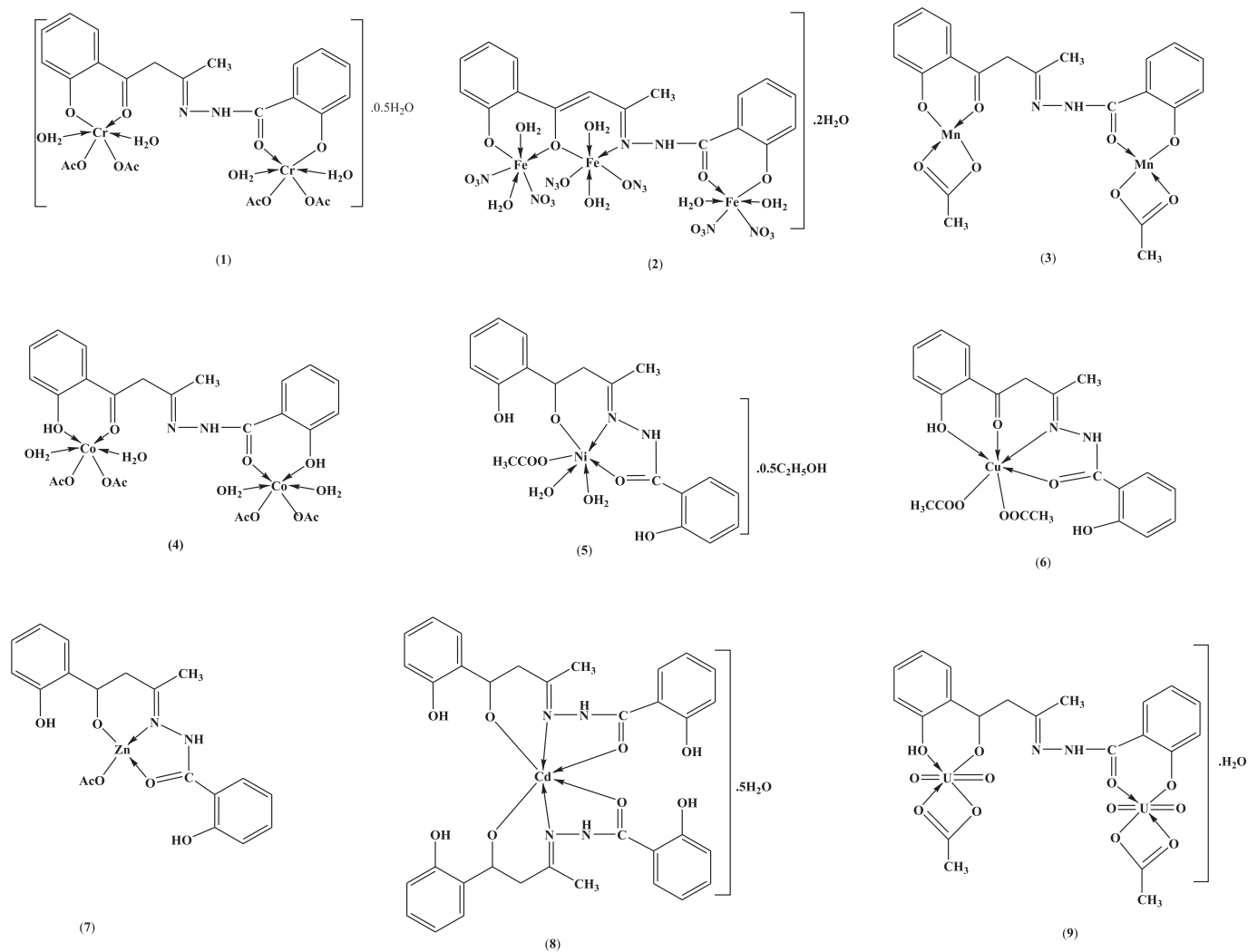
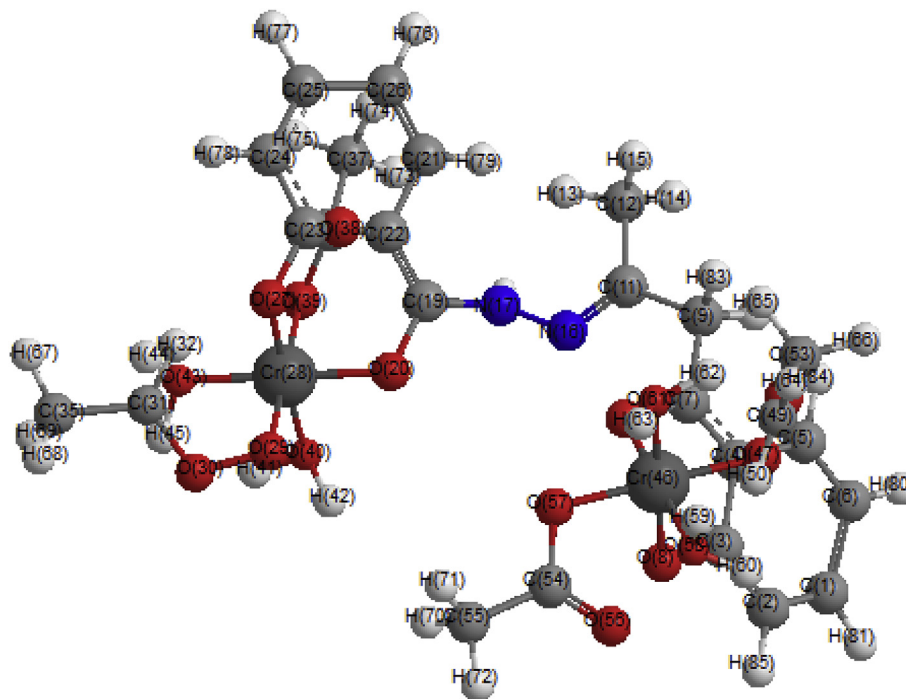**Fig. 8.** Representative structures of metal complexes of H₃L ligand.

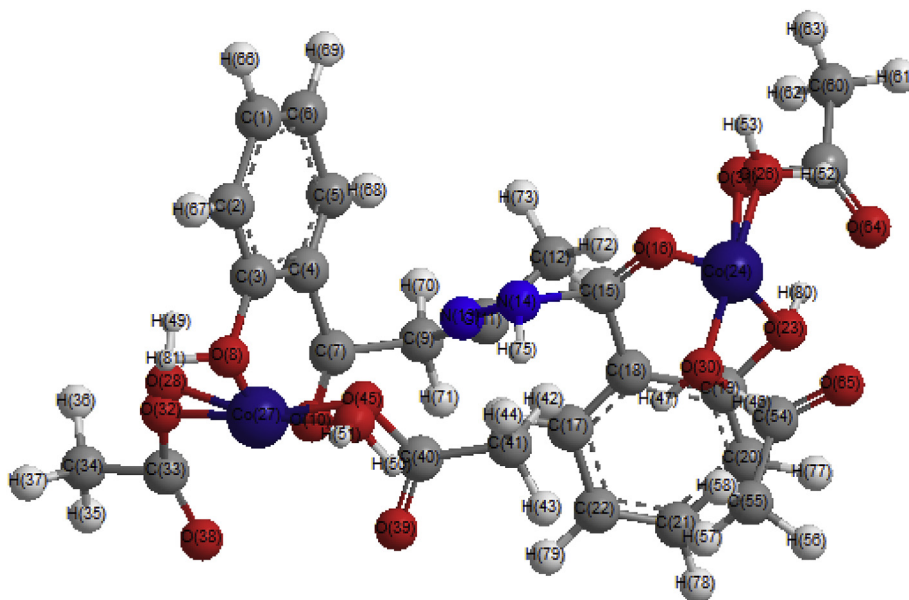**Fig. 9.** Molecular modeling of [(HL)Cr(OAc)₄(H₂O)₄]. 0.5H₂O **1**.

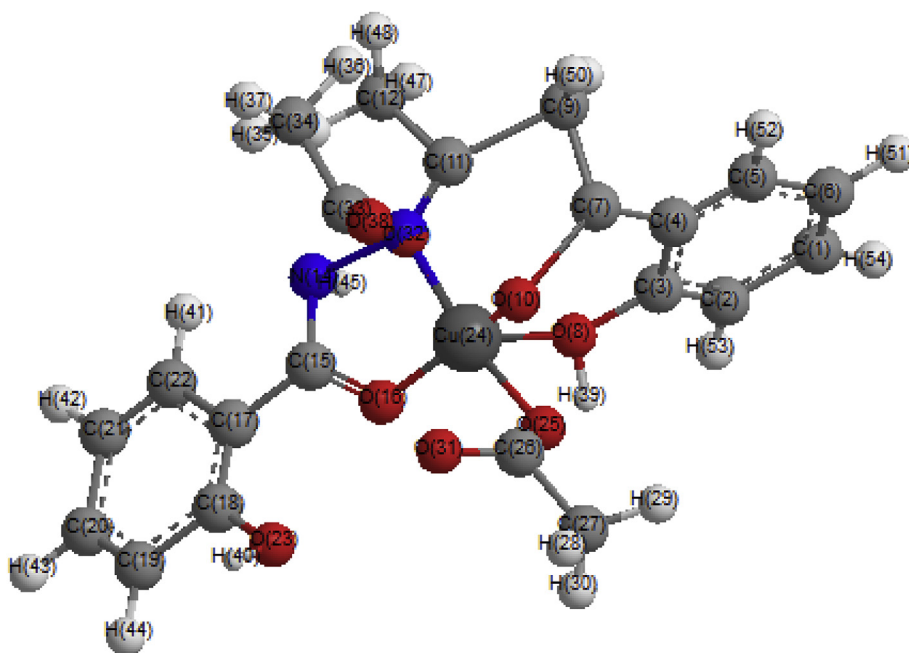**Fig. 10.** Molecular modeling of [(H₃L)Co₂(OAc)₄(H₂O)₄] **4**.

Fig. 11. Molecular modeling of [(H₃L)Cu(OAc)₂] **6**.

was accompanied by increasing the M—N bond strength.

5. Antimicrobial activity

The Schiff base ligand and its metal complexes were screened for antimicrobial activity against Gram positive bacteria (*S. aureus*, G+1 and *B. subtilis, G+2*), Gram negative bacteria (*S. typhimurium, G-1* and *E. coli, G-2*) and fungi (*C. albicans, Y* and *A. fumigates, F*) and the results are listed in Table 10. The ligand is high active against *S. aureus*, G+1 and *S. typhimurium, G-1*, whereas intermediate or low active against other microorganisms under investigation. In-hibition was found to increase with increasing concentration of metal complex as shown in Table 9.

However, the activity of the current complexes toward the screened microorganisms could be summarized: complex **4** showed high activity towards *Bacillus subtilis* (G+2) and *Candida albicans (Y)*, while complexes **5** and **8** showed high activity toward *Staphylococcus aureus* (G+1) and complex **8** showed high activity towards *Bacillus subtilis* (G+2). Whereas, complexes: **5** and **6** showed high activity against *Candida albicans* (Y). Complexes **2**, **6** and **9** showed moderate activity towards *Bacillus subtilis* (G+2). Complexes **4**, **5** and **8** showed moderate activity towards *Salmonella typhimurium* (G-1). But complexes **7**, **8** and **9** showed moderate activity towards *Candida albicans* (Y).

Stability of the complex play again an important role on bio-logical activity of the current complexes as deduced from the linear
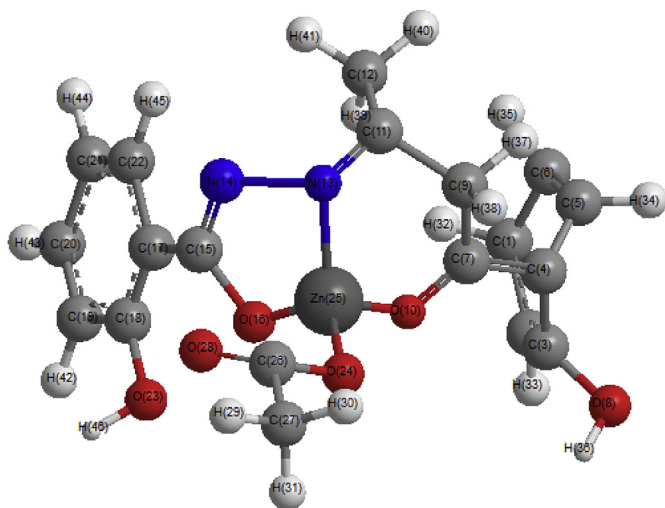
Fig. 12. Molecular modeling of [(H$_2$L)Zn(OAc)] **7**.

relationships of the IR data versus the data in Table 9. The negative slopes of the stretching vibrational frequencies of the carbonyl or azomethine group (higher hypsochromic shift relevant to higher Lewis acid-base indicators) versus the biological activity against either Y1 or G+2, $\nu_{C=O}/cm^{-1} = 1603 - 109.5Y1$, r = 0.97, n = 6 except **3**, **4**, **5** and $G^{+2} = 18.02 - 0.011\nu_{C=N}/cm^{-1}$, r = 996, n = 4 except **1**, **2**,

6, **8** and **9** complexes.

It was noticed in elucidating the microbial activity to find a correlation of Frontier orbitals energy HOMO, LUMO and E$_{gap}$, with the biological activity of the screened organisms yield: E$_{HOMO}$/eV = −5.059−4.417G+2, r = 0.99, n = 4 except **1**, **2**, **7** and **9** complexes. The negative slope reveals decreasing the biological activity toward gram positive with the increasing of E$_{HOMO}$ (less stability). This interpretation emphasized by the positive slope of the linear correlation of E$_{gap}$, that relevance to stability of complexes against the biological activity toward the current microorganism: E$_{gap}$/eV = 5.145 + 4.772G-1, r = 0.981, n = 5; i.e., the biological activity enhanced towards gram negative and gram positive with the increasing of complex stability. Furthermore, the extent of electrondonating properties of ligand to the metal ion (*ED*) is linearly correlated with a positive slope versus the data in Table 9: *ED*/Kcal.mol^{-1} = 5.146 + 4.77, G-1 r = 0.98 n = 5 and *ED* (y) = −1.642e +05 + 7.267e+05G+1, r = 0.998, n = 4 except complex **1**. The enhancement of bacterial activity of ligand after chelation can be attributed to the positive charge of metal ion that partially or completely neutralized by the ligand anion and/or shared with donor atoms present on ligand and possible π-electron delocalization over the whole chelate ring. This, in turn, increases the lipophilic character of the metal chelate and favors its permeation through the lipid layers of the bacterial membranes resulting in interference with normal process. This interpretation supported by the positive slope of the linear correlations of the dipole moment against the data in Table 9: Dipol moment

Table 7
Structural parameters of the free ligand and its metals complexes, calculated, on the basis of *PM3* level using semi-empirical implemented on Hyperchem *7.52* program, the values in the paranthesis calculated by means DFT using the B3LYP and the basis set 6-31G level provides by the Gaussian 09 program.

No.	Complexes	Total energy	Dipol moment	Bonding energy	Heat of formation	Electronic energy	Neuclear energy	Energy HOMO	Energy LUMO	E$_{gap}$	ED
	H$_3$L	−86617.27	3.617	−4227.84	−24.841	−606177.00	519559.75	−9.180 (−5.21)	−0.713 (−1.659)	8.467 (3.55)	−
1	[(HL)Cr(OAc)$_4$(H$_2$O)$_4$].0.5H$_2$O	−207810.37	17.27	−8132.06	−719.39	−2133073.75	1925263.38	5.083	1.720	3.363	121193.10
2	[(HL)Mn$_2$(OAc)$_2$]	−144023.59	6.121	−5678.60	−209.995	−1172298.75	1028296.69	−7.830	−1.059	6.771	57406.32
3	[(L)Fe$_3$(NO$_3$)$_6$(H$_2$O)$_6$].2H$_2$O	−133959.59	18.130	−7289.73	412.731	−3960091.00	3646131.50	−4.502	−2.848	1.654	47342.32
4	[(H$_3$L)Co$_2$(OAc)$_4$(H$_2$O)$_4$]	−232707.66	14.200	−8436.58	−1009.110	−2298046.75	2065339.00	−8.191	−1.016	7.175	146090.39
5	[(H$_3$L)Ni(OAc)(H$_2$O)$_2$].0.5C$_2$H$_5$OH	−145508.63	11.140	−5692.53	−494.103	−1186623.50	1041114.93	−8.073	−0.866	7.207	58891.36
6	[(H$_3$L)Cu(OAc)$_2$]	−154141.36	7.898	−5784.73	−266.628	−1364334.63	12101193.25	−7.047	−0.762	6.285	67524.09
7	[(H$_3$L)Zn(OAc)]	−107004.65	5.129	−4905.51	−106.237	−818249.31	711244.62	−8.676	−1.043	7.633	20387.38
8	[(H$_3$L)$_2$Cd].5H$_2$O	−174482.77	6.174	−8583.23	−46.308	−1925009.25	1750526.50	−8.283	−0.555	7.728	87865.50

Table 8
The selected bond lengths of the optimized structures of transition metal complexes.

| Atoms	Charges of atoms in complexes								
	H$_3$L	1	2	3	4	5	6	7	8
C(3)−O(8)	1.364	1.373	1.355	1.359	1.364	1.350	1.383	1.350	1.360
C(7)=O(10)	1.216	1.379	1.388	1.502	1.497	1.306	1.274	1.286	1.432
C−O$_{(OAc)bi.}$	−	−	1.265	−	−	−	−	−	−
C−O$_{(OAc)mo.}$	−	1.393	−	−	1.365	1.327	1.328	1.318	−
C(11)=N(13)	1.301	1.320	1.320	1.514	1.320	1.338	1.346	1.362	1.519
C(18)or(19)- O(22)or (23)	1.368	1.378	1.325	1.359	1.363	1.357	1.354	1.245	−
C(14)or (15)=O (15)or(16)	1.249	1.350	1.265	1.496	1.497	1.262	1.228	1.286	1.499
M−O(8)	−	1.933	1.860	1.896	1.896	−	2.090	2.304	2.209
M=O(10)	−	1.722	1.866	1.896	1.883	1.828*	1.969	2.069	−
M−O$_{(OAc)mo.}$	−	1.892	−	−	1.890	1.838	1.869	1.997	−
M=N(13)	−	−	−	1.912	−	1.837	1.955	2.046	2.227
M−O(22)or(23)	−	1.821	1.883	1.900	1.889	−	−	−	−
M=O(15)or(16)	−	1.865	1.847	1.895	1.886	1.858	2.078	−	2.209
M−O$_{H2O,EtOH}$	−	2.008	−	1.899	1.890	2.045	−	−	−
M−O$_{(NO3)}$	−	−	−	1.901	−	−	−	−	−
M−O$_{(OAc)bi.}$	−	−	1.916	−	−	−	−	−	−

HOMO H$_3$L

LUMO H$_3$L
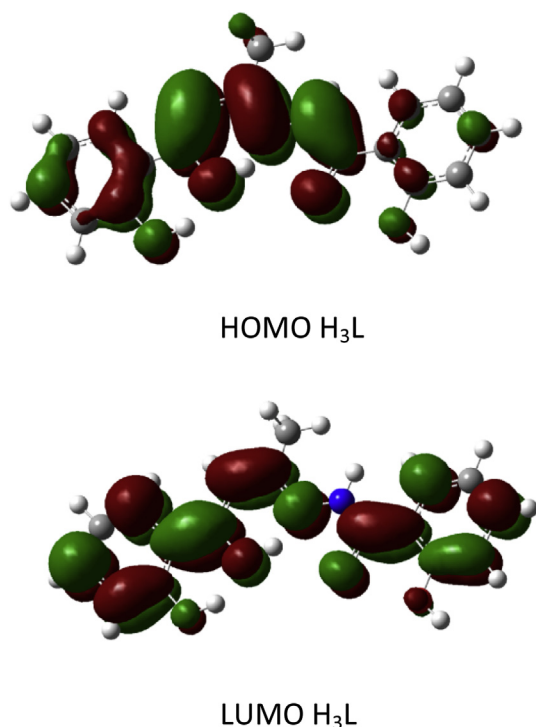
Fig. 13. The contour plots of the frontier orbitals of free Schiff base ligand, H$_3$L calculated by means of Density DFT using the B3LYP and the basis set 6-31G level, provides by the Gaussian 09 program.

$(y) = -3.633 + 24.043 \text{ G+2}, r = 0.986 \text{ n} = 5$ and Dipol moment $= -16.29 + 40.67 \text{ F}_1, r = 0.97, \text{n} = 5.$

6. Antitumor activity

The anticancer activity of the Schiff base ligand and its Ni(II) and Cu(II) complexes was determined *in vitro* against human cancer cell line liver Carcinoma (HEPG2). Table 10 schedules the values of IC$_{50}$,

Table 10
Antitumor activity of the Schiff base ligand and its nickel(II) and copper(II) complexes against HepG2 cell line.

Compound	IC$_{50}$ (μg/ml)
H$_3$L	205
[(H$_3$L)Ni(OAc)(H$_2$O)$_2$].0.5C$_2$H$_5$OH **5**	24.80
[(H$_3$L)Cu(OAc)$_2$] **6**	10.20
Doxorubicin	0.47

IC$_{50}$ = inhibition concentration 50%.

compared with the standard drug doxorubicin. The ligand and its complexes showed lower activity and the order of activity is as follows: Cu(II) complex > Ni(II) complex > H$_3$L ligand. The difference in activity of the complexes indicates that the type of ion may be the reason for the different anticancer activity [60].

7. Conclusion

A new Schiff base ligand was synthesized and characterized. Mononuclear complexes were obtained in case of Cu(II), Ni(II), Zn(II) and Cd(II) ions. The coordination sites of Cu(II) complex is O,N,O,O sites while Ni(II) and Zn(II) complexes coordination sites are O,N,O sites and Cd (II) complex showed M:L; 1:2 molar ratio.

Binuclear complexes were obtained in case of Cr(II), Mn(II), Co(II) and UO$_2$(VI) ions. The coordination sites is O,O,O,O sites. Trinuclure complex in case of Fe (III) complex. The coordination sites of is O,O,N,O,O sites. The geometrical structures were proposed for metal complexes such as octahedral structure for all complexes except Mn(II) and Zn(II) complexes showed tetrahedral arrangement. Kinetic parameters of the thermal decomposition stages have been evaluated using Coats−Redfern equations. The molecular parameters of the ligand and its metal complexes have been calculated and correlated with the experimental data. The antimicrobial activity of the ligand and its complexes were investigated. The antimicrobial activity of the ligand and its complexes was investigated. The antitumor activity of the ligand and its Ni(II) and Cu(II) complexes was investigated against HepG2 cell line.

Table 9
Antimicrobial activity of the free ligand (H$_3$L) and some of its metal complexes.

Organism	Mean* of zone diameter, nearest whole mm.											
	Gram - positive bacteria				Gram - negative bacteria				Yeasts and Fungi**			
	Staphylococcus aureus (ATCC 25923)		*Bacillus subtilis* (ATCC 6635)		*Salmonella typhimurium* (ATCC 14028)		*Escherichia coli* (ATCC 25922)		*Candida albicans* (ATCC 10231)		*Aspergillus fumigatus*	
Sample	Concentration											
	1 mg/ml	0.5 mg/ml	1 mg/ml	0.5 mg/ml	1 mg/ml	0.5 mg/ml	1 mg/ml	0.5 mg/ml	1 mg/ml	0.5 mg/ml	1 mg/ml	0.5 mg/ml
H$_3$L	24 H	19 H	11 L	8 L	25 H	20 H	–	–	15 I	12 I	18 I	15 I
1	10 L	8 L	10 L	14 I	–	–	–	–	13 I	9 L	–	–
2	–	–	14 I	13 I	–	–	–	–	10 L	7 L	-	-
3	–	–	–	–	–	–	–	–	18 H	16 I	-	-
4	15 I	12 I	25 H	21 H	17 I	14 I	14 I	10 I	31 H	27 H	–	–
5	28 H	24 H	23 I	19 H	14 I	12 I	17 I	15 I	27 H	24 H	25 H	23 H
6	11 L	8 L	16 I	13 I	9 L	7 L	20 I	15 I	26 H	22 H	21 I	18 H
7	9 L	8 L	22 I	20 H	–	–	–	–	20 I	17 I	20 I	18 H
8	28 H	25 H	26 H	20 H	19 I	17 I	25 I	19 H	13 I	10 I	21 I	18 H
9	–	–	19 I	16 I	–	–	–	–	22 I	18 I	22 I	20 H
Control#	35	26	35	25	36	28	38	27	35	28	37	26

- No effect.
L: Low activity = Mean of zone diameter ≤1/3 of mean zone diameter of control.
I: Intermediate activity = Mean of zone diameter ≤2/3 of mean zone diameter of control.
H: High activity = Mean of zone diameter >2/3 of mean zone diameter of control.
#: Chloramphencol in the case of Gram-positive bacteria, cephalothin in the case of Gram-negative bacteria and cycloheximide in the case of fungi. *Calculate from three values.

References

[1] S.M.E. Khalil, J. Coord. Chem. 56 (2003) 1013.
[2] K.A.R. Salib, M.F. Ishak, M.A. El-Behairy, H.F. Abd El-Halim, Synth. React. Inorg. Met.-Org. Chem. 33 (2003) 1667.
[3] M. Shebl, Spectrochim. Acta A 117 (2014) 127.
[4] M. Shebl, S.M.E. Khalil, Saleh A. Ahmed, H.A.A. Medien, J. Mol. Struct. 980 (2010) 39.
[5] T.M. Sorrell, Tetrahedron 45 (1989) 3.
[6] L.F. Lindoy, Pure Appl. Chem. 61 (1989) 1575.
[7] M.F. Loncin, J.F. Desreux, E. Merciny, Inorg. Chem. 25 (1986) 2646.
[8] P.A. Vigato, S. Tamburini, D.E. Fenton, Coord. Chem. Rev. 106 (1990) 25.
[9] M.S. Refat, I.M. El-Deen, Z.M. Anwer, S. El-Ghol, J. Mol. Struct. 920 (2009) 149.
[10] M. Rajasekar, S. Sreedaran, R. Prabu, V. Narayanan, R. Jegadeesh, N. Raaman, A.K. Rahiman, J. Coord. Chem. 63 (2010) 136.
[11] C.J. Dhanaraj, M.S. Nair, J. Coord. Chem. 62 (2009) 4018.
[12] Y.-T. Liu, G.-D. Lian, D.-W. Yin, B.-J. Su, Spectrochim. Acta A 100 (2013) 131.
[13] S.K. Sridhar, S.N. Pandeya, J.P. Stables, A. Ramesh, Eur. J. Med. Chem. 16 (2002) 129.
[14] S.N. Pandeya, P. Yogeeswari, D. Sriram, De. E. Clercq, C. Pannecouque, M. Witvrouw, Chemotherapy 45 (1999) 192.
[15] K.H. Reddy, P.S. Reddy, P.R. Babu, Trans. Met. Chem. 25 (2000) 154.
[16] P. Tarasconi, S. Capacchi, G. Pelosi, M. Corina, R. Albertini, A. Bonati, P.P. Dall'Aglio, P. Lunghi, S. Pinelli, Bioorg. Med. Chem. 8 (2000) 157.
[17] K. Verma, S.N. Pandeya, U.K. Singh, S. Gupta, P. Prashant, A.G. Bhardwaj, Int. J. Pharm. Sci. 1 (2009) 357.
[18] A. Prakash, D. Adhikari, Int. J. Chem. Tech. Res. 3 (2011) 1891.
[19] E.J. Baran, J. Inorg. Biochem. 80 (2000) 1.
[20] F. Velde, I.W.C.E. Arends, R.A. Sheldon, J. Inorg. Biochem. 80 (2000) 81.
[21] X.D. Zhu, C.G. Wang, Y.L. Dang, H.B. Zhou, Z.S. Wu, Z.J. Liu, D.L. Ye, Q.C. Zhou, Synth. React. Inorg. Met.-Org. Chem. 30 (2000) 625.
[22] R. Herzfeld, P. Nagy, Spectrosc. Lett. 32 (1999) 57.
[23] S.M.E. Khalil, K.A. Bashir, J. Coord. Chem. 55 (2002) 681.
[24] L. Liu, M.S. Alam, D.-U. Lee, Bull. Korean Chem. Soc. 33 (2012) 3361.
[25] H.A. Flaschka, EDTA Titration, second ed., Pergamon Press, 1964, p. 81.
[26] A.I. Vogel, Textbook of Quantitative Inorganic Analysis, fourth ed., Longman, London, 1978.
[27] T.S. West, Complexometry with EDTA and Related Reagents, third ed., DBH Ltd., Pools, 1969.
[28] F.E. Mabbs, D.I. Machin, Magnetism and Transition Metal Complexes, Chapman and Hall, London, 1973.
[29] A.W. Bauer, W.W.M. Kirby, J.C. Sherris, M. Turck, Am. J. Clin. Pathol. 45 (1966) 493.
[30] D.C. Gross, S.E. De Vay, Physiol. Plant Pathol. 11 (1977) 13.
[31] T. Mosmann, J. Immunol, Methods 65 (1983) 55—63;

(b) A.P. Wilson, in: J.R.W. Masters (Ed.), Cytotoxicity and Viability Assay in Animal Cell Culture: a Practical Approach, third ed., Oxford University Press, 2000.
[32] A.A.A. Emara, A.A.A. Abou-Hussen, Spectrochim. Acta (A) 64 (2006) 1010.
[33] V. Gutmann, The Donor-acceptor Approach Molecular Interactions, Plenum Press, New York, London, 1978.
[34] O.M.I. Adly, A. Taha, J. Mol. Str. 1038 (2013) 250.
[35] M. Shebl, J. Coord. Chem. 69 (2016) 199.
[36] A. Taha, Spectrochim. Acta (A) 59 (2003) 1611.
[37] S.M.E. Khalil, Synth. React. Inorg. Met.-Org. Chem. 31 (2001) 417.
[38] S.M.E. Khalil, M. Shebl, F.S. Al-Gohani, Acta Chim. Slov. 57 (2010) 716.
[39] G.M. Abu El-Reash, O.A. El-Gammal, A.H. Radwan, Spectrochim. Acta A 121 (2014) 259.
[40] M. Shebl, M.A. El-ghamry, S.M.E. Khalil, M.A.A. Kishk, Spectrochim. Acta A 126 (2014) 232.
[41] M. Shebl, S.M.E. Khalil, Monatsh. Chem. 146 (2015) 15.
[42] M. Shebl, S.M.E. Khalil, A. Taha, M.A.N. Mahdi, Spectrochim. Acta A 113 (2013) 356.
[43] O.M.I. Adly, Spectrochim. Acta (A) 95 (2012) 483.
[44] S.P. Mcglynn, J.K. Smith, W.C. Neely, J. Chem. Phys. 35 (1961) 105.
[45] L.H. Jones, Spectrochim. Acta A 10 (1958) 395.
[46] A.A. El-Asmy, O.A. El-Gammal, H.A. Radwan, Spectrochim. Acta A 76 (2010) 496—501.
[47] W.J. Geary, Coord. Chem. Rev. 7 (1971) 81.
[48] A. Taha, A.A.M. Farag, O.M.I. Adly, N. Roushdyd, Magdy Shebl, H.M. Ahmed, J. Mol. Struct. 1142 (2017) 66—72.
[49] O.M.I. Adly, A. Taha, S.A. Fahmy, J. Mol. Struct. 1083 (2015) 450.
[50] M. Gaber, N.A. El-Wakiel, H. El-Ghamry, S.K. Fathalla, J. Mol. Struct. 1076 (2014) 251.
[51] X. Zhang, Y. Zhang, L. Yang, P.R. China, R. Yange, D. Jin, Synth. React. Inorg. Met.-Org. Chem. 58 (2000) 45—54.
[52] O.M.I. Adly, A. Taha, S.A. Fahmy, J. Mol. Struct. 1054—1055 (2013) 239.
[53] F.A. Cotton, G. Wilkinson, Advanced Inorganic Chemistry, a Comprehensive Text, fourth ed., John Wiley & Sons, New York, 1986.
[54] O.M.I. Adly, A.A.A. Emara, Spectrochim. Acta (A) 132 (2014) 91.
[55] N.N. Greenwood, A. Earnshaw, Chemistry of the Elements, Pergamon Press, New York, 1984.
[56] N.M. El-Metwally, I.M. Gabr, A.A. El-Asmy, A.A. Abou-Hussen, Transit. Met. Chem. 31 (2006) 71.
[57] B. Jezowska-Trzebiatowska, J. Lisowski, A. Vogt, P. Chemielewski, Polyhedron 7 (1988) 337.
[58] C.R. Vinodkumar, M.K.M. Nair, P.K. Radhakrishnan, J. Therm. Anal. Cal. 61 (2000) 143.
[59] A.H.M. Siddaligaiah, S.G. Naik, J. Mol. Str. Theochem. 582 (2002) 129.
[60] N. El-wakiel, M. El-keiy, M. Gaber, Spectrochim. Acta Part A 147 (2015) 117.